

Article

Experimental Modeling of CO₂ Sorption/Desorption Cycle with MDEA/PZ Blend: Kinetics and Regeneration Temperature

Quentin Wehrung^{1,*}, Enrico Destefanis¹, Caterina Caviglia¹, Davide Bernasconi¹, Linda Pastero¹, Marco Bruno¹, Andrea Bernasconi¹, Alex Magnetti Vernai², Alice Di Rienzo² and Alessandro Pavese¹

¹ Earth Science Department, University of Turin, Via Valperga Caluso, 35, 10125 Torino, Italy; enrico.destefanis@unito.it (E.D.); caterina.caviglia@unito.it (C.C.); davide.bernasconi@unito.it (D.B.); linda.pastero@unito.it (L.P.); marco.bruno@unito.it (M.B.); andrea.bernasconi@unito.it (A.B.); alessandro.pavese@unito.it (A.P.)

² Ecospray Technologies Srl, Via Circonvallazione, 14/14A, 15050 Alzano Scrivia, Italy; magnetti@ecospray.eu (A.M.V.); alice.dirienzo@ecospray.eu (A.D.R.)

* Correspondence: quentin.wehrung@unito.it; Tel.: +39-33663281762

Abstract: CO₂ sorption–desorption cycles with a methyldiethanolamine (MDEA)/piperazine (PZ) blend have been performed with a rotoevaporator. Similar to other CO₂ separation technologies, the heating involved in MDEA/PZ solvent regeneration is the most energy-intensive step in the overall CO₂ separation process. Thus, this study investigated the desorption kinetics under low-pressure (<200 mbar) and low-temperature conditions in the range from 308 to 363 K with the aim of reducing costs. The CO₂ desorption time to unload the samples from ~2.35 mol/kg to below the threshold of 1 mol/kg was reduced from 500 s at 333 K to 90 s at 363 K. The Avrami–Erofojev model was found to fit the experimental kinetic data accurately. The Arrhenius law calculations provided an activation energy of the CO₂ desorption process equal to 76.39 kJ/mol. It was demonstrated that the combination of a pressure reduction and the increase in temperature resulted in an enhancement of the desorption kinetics, especially at low temperatures. The combined effect of these two factors resulted in higher desorption kinetics compared to the individual effects of either factor alone. Solvent regeneration at a low temperature was demonstrated to be a valid option when coupled with pressure reduction.

Keywords: amine blend; CO₂ capture; solvent regeneration; vacuum system; roto-evaporator



Citation: Wehrung, Q.; Destefanis, E.; Caviglia, C.; Bernasconi, D.; Pastero, L.; Bruno, M.; Bernasconi, A.; Magnetti Vernai, A.; Di Rienzo, A.; Pavese, A. Experimental Modeling of CO₂ Sorption/Desorption Cycle with MDEA/PZ Blend: Kinetics and Regeneration Temperature.

Sustainability **2023**, *15*, 10334.

<https://doi.org/10.3390/su151310334>

su151310334

Academic Editor: Yuanbo Zhang

Received: 4 May 2023

Revised: 21 June 2023

Accepted: 28 June 2023

Published: 29 June 2023



Copyright: © 2023 by the authors. Licensee MDPI, Basel, Switzerland. This article is an open access article distributed under the terms and conditions of the Creative Commons Attribution (CC BY) license (<https://creativecommons.org/licenses/by/4.0/>).

1. Introduction

Stationary point sources such as fossil fuel-fired power plants, industrial processes like cement production, and waste incinerators represent the largest contributors to CO₂ emissions, thereby exerting a significant impact on global climate change. Stationary point sources are collectively responsible for ~65% of the global greenhouse gas emissions [1]. Chemical ab-/adsorption is the most widely used technique of CO₂ removal from flue gas. Utilizing an amine-based solvent offers a post-combustion CO₂ capture method that distinguishes itself from others due to its high selectivity for carbon dioxide and its ability to regenerate the solvent. These advantages make it a distinct and advantageous strategy. Additionally, both ab-/adsorption (hereafter “sorption”) and regeneration columns can be retrofitted to plants, thus making amine-based capture among the most common methods for capturing CO₂ from power plants [2]. In the contemporary era, amine-based technology has achieved a high degree of maturity and is the only method of CO₂ capture that has been applied so far at a wholesale scale for natural gas processing, methane upgrading, hydrogen purification and removal of CO₂ from industrial flue gases [3]. Capturing CO₂ through amine is deeply affected by the choice of the solvent, a decision that influences the resulting reaction kinetics, the energy of regeneration and the degradation of the active solution [4]. Among the numerous solvents used as a CO₂ sorbent, the present study focuses on the

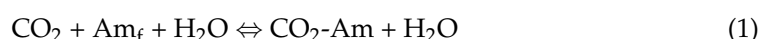
piperazine (PZ)-activated aqueous methyldiethanolamine (MDEA) solution. This blend (MDEA/PZ) offers advantages over the use of monoethanolamine (MEA) and MDEA alone due to its resistance to thermal and chemical degradation, as well as its high CO₂ capture capacity at typical sorption/stripping conditions [5,6]. However, MDEA exhibits a slower reaction rate with CO₂ compared to other alkanolamines. Consequently, MDEA solutions are commonly activated via the incorporation of a reaction kinetics promoter, such as PZ [7], to enhance the reaction rate. Nonetheless, the significant cost associated with sorbent regeneration remains one of the major hurdles in chemical sorption processes. Typically, high temperatures ranging from 383 to 453 K [8] are employed for desorption, which contributes to the overall expense. In order to address this issue, scholars have explored alternative approaches such as a membrane vacuum system [9,10] in order to minimize the desorption temperature as much as possible. This innovative technique has the potential to reduce costs by employing lower temperatures during the regeneration process.

While most of the recent amine-based CO₂ capture studies focus on sorption and/or its thermodynamics, primarily via software simulations, e.g., with Aspen programs [11–15], comparatively little attention has been paid to the reaction kinetics of the CO₂ sorption and desorption cycles with the MDEA/PZ blend [16]. This aspect plays an important role in obtaining further insights into the CO₂ sorption/desorption mechanism for the purpose of boosting enhancements of the related technology [17].

In this light, the present study aims to improve the sustainability of the MDEA/PZ-based CO₂ sorption–desorption/regeneration cycle. Specifically, our efforts are directed towards the establishment of a correlation between desorption reaction kinetics and relatively low desorption/regeneration temperatures ranging from 308 to 363 K. In addition, we explore the utilization of low pressure to force desorption, while preserving the active solution from degradation to as great an extent as is possible.

General Kinetic Mechanism

The reaction mechanism behind CO₂ sorption by a MDEA/PZ mixture was described by [18]. Ref. [19] argued that, in an aqueous MDEA solution, bicarbonate formation and MDEA protonation are rate-limiting for the reaction with CO₂. Moreover, [20] showed that the carbamate PZCOO[−] and dicarbamate PZ(COO[−])₂ formation are rate-limiting in a solvent containing PZ. Amine-driven CO₂ capture reaction equilibrium is formalized by the equation below:



where Am_f and CO₂-Am are CO₂-free amine and CO₂-sorbed amine, respectively.

A fraction of CO₂ is sorbed onto amine, whereas another fraction remains physically dissolved through the solvent as a function of the weak chemical bonding of carbon dioxide with the solvent functional groups [21]. Physical sorption [4] varies with the CO₂ solubility, the CO₂ partial pressure and the temperature of sorption [22]. Chemical sorption depends upon the stoichiometry of the CO₂/solvent functional groups reaction and the concentration of the reagents. In the present study, we use the term “desorption of CO₂” to signify the induced process of breaking bonds and allowing carbon dioxide to leave the amine blend, an undertaking with the potential to regenerate the sorption capacity of the latter, and to prevent the occurrence of degradation via the decomposition of the CO₂–amine system into carbamate/bicarbonate [17,23].

2. Materials and Methods

2.1. Chemical Reagents

The experiments were performed with an industrial amine blend aqueous solution (AmPZ hereafter) with a molarity of 3.73 mol/kg (methyldiethanolamine 28.11 wt.%, piperazine 11.85 wt.%). CO₂ was provided by Gruppo Sapio Srl at a purity of 99.9 %. The amine blend aqueous solution is selected for its amine molarity in the optimal range of CO₂ sorption efficiency [24]. MDEA, also known as 2,2'-Methyliminodiethanol or *N,N*-Bis(2-

hydroxyethyl)methylamine, has a chemical formula of $C_5H_{13}NO_2$. It is a tertiary amine compound with a molar mass of 119.16 g/mol and a density of 1.038 g/cm³. Piperazine, or 1,4-Diazacyclohexane, is a secondary diamine with a chemical formula of $C_4H_{10}N_2$. It has a molar mass of 86.14 g/mol and a density of 1.1 g/cm³. Its topological formulae are shown in Figure 1.

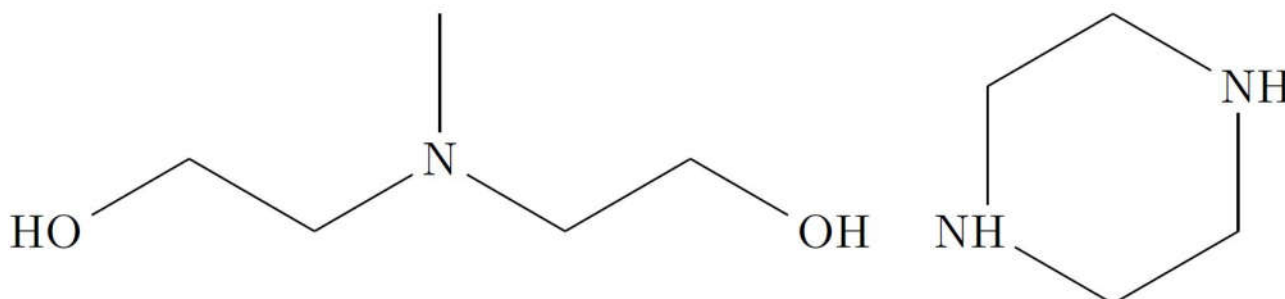


Figure 1. Topological formulas for MDEA (left) and PZ (right).

2.2. Laboratory Equipment

The experiments were designed using a roto-evaporator IKA 3 RV eco, equipped with a heating bath up to 373 K, a speed range of 20 to 300 rpm, and a high-efficiency condenser with 1500 cm² cooling surface. The gas–liquid interfacial area was determined geometrically such as $A = 339.7$ cm². A Welch pump was provided by Gardner Denver. CO₂ pressure and flows were measured and controlled by a Bronkhorst modular system, composed of: a mass stream (“valve” hereafter) (MFC D-6321), with a maximum flow range of 2 L_n/min CO₂ and accuracy $\pm 1.0\%$ RD plus $\pm 0.5\%$ FS; a low Δp (“flow meter” hereafter) F101E (max flow range of 3 L_n/min CO₂ and accuracy $\pm 1.0\%$ FS); and an El-Press (“pressure meter” hereafter) P-700 digital electronic backward pressure controller calibrated between 0.28 and 1.7 bar for the measurement of the distiller pressure. A digital PC board provides self-diagnostics, alarm and counter functions, digital communication (RS232), and remotely adjustable control settings, and an onboard interface based on the FLOW-BUS protocol makes it possible to communicate via a multi-bus system. The combination and operating sequence of the Bronkhorst devices depend on whether the sorption or desorption mode is being run, as we shall discuss below. Sorption/desorption data acquisition was performed every 5th second. pH and EC (electrolytical conductivity, $\mu\text{S}/\text{cm}$) of the amine samples were measured by a Hanna HI H-ORP meter and a Mettler Toledo Five Easy EC-meter, respectively. The samples’ masses were measured with a precision of $\pm 0.1\%$.

2.3. Experimental Procedure

Each experiment was carried out on 100 g AmPZ, prepared using the chemical reagents mentioned above. Preliminary tests proved that ten consecutive CO₂ sorption (6 min)/desorption (10 min) cycles were sufficient to describe the capture–release cycle of the active solution. In particular, the sorption rate falls below 50% at $t > 6$ min (low efficiency regime), whereas at $t = 10$ min, desorption has achieved its completion. The background of the experimental setup was estimated by sorption/desorption blank cycles, using the solutions described in Section 2.3.1. The same “distiller” was used as a hybrid reactor for both sorption and desorption steps, as shown in Figure 2, in order to eliminate any handling of the solution and reduce subsequent weight losses. Both the sorption/desorption apparatus and the related procedures are reported in Sections 2.3.2 and 2.3.3, respectively.

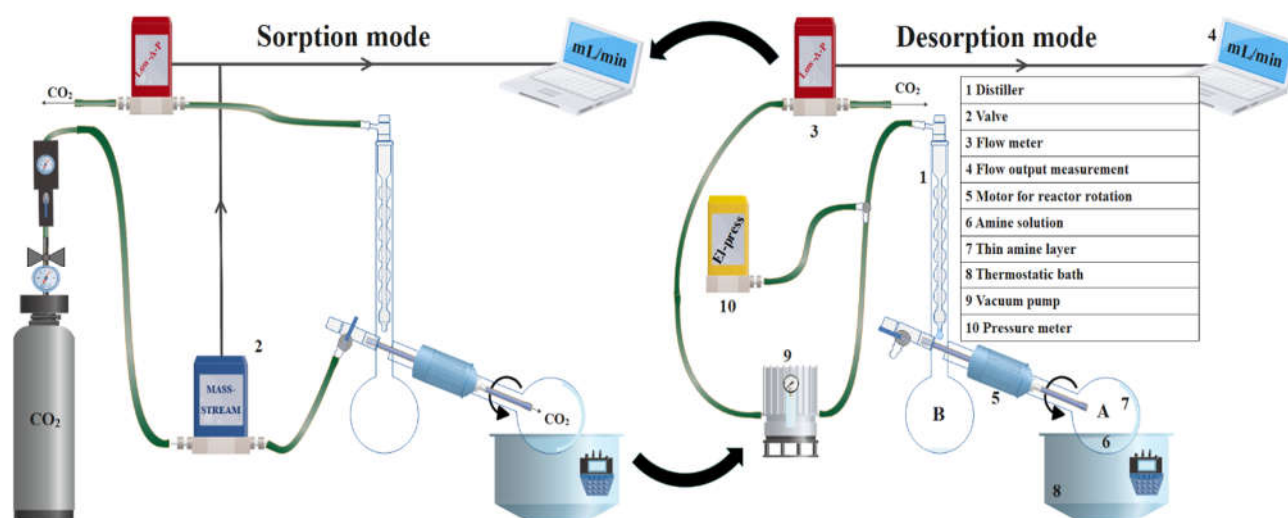


Figure 2. Experimental setup during the sorption (left) and desorption (right) cycles.

The experimental parameters are laid out in Table 1. Experimental runs were performed, changing desorption temperature in the range of 308 to 363 K, and keeping pressure <200 mbar. An additional suite of runs was carried out at 1 atm, sharing the same thermal interval mentioned above to bring to light the effect of pressure reduction.

Table 1. Summary of the experimental parameters.

Experiments Number	Initial Mass (g)	Mixing Velocity (rpm)	Cycles (Count)	Time (s)	Sorption		Desorption			
					Temp. (K)	CO ₂ Flow (L/min)	Time (s)	Temp. (K)	Pressure (mbar)	
A	1	100	120	10	360	308	1	600	308	150 ± 20
	2	100	120	10	360	308	1	600	323	150 ± 20
	3	100	120	10	360	308	1	600	333	150 ± 20
	4	100	120	10	360	308	1	600	343	150 ± 20
	5	100	120	10	360	308	1	600	353	150 ± 20
	6	100	120	10	360	308	1	600	363	150 ± 20
B	1	100	120	2	360	308	1	600	323	atm
	2	100	120	2	360	308	1	600	333	atm
	3	100	120	2	360	308	1	600	343	atm
	4	100	120	2	360	308	1	600	353	atm
	5	100	120	2	360	308	1	600	363	atm

2.3.1. Blank Experiments

Several series of “blank” sorption/desorption experiments were performed in the empty reactor, using the procedures described in the ensuing sections, in order to correctly calibrate the setup. The average sample weight loss (m_{loss}) due to pump suction over ten desorption steps was measured with 100 g AmPZ for temperatures ranging from 308 to 363 K. m_{loss} was observed to be weakly sensitive to T and estimated to be about 0.6 g/cycle. Another series of “blank” experiments was performed in the empty reactor in sorption mode as a function of the inflow in order to calibrate gas valve and flow meter measurements. A linear proportionality was observed to hold between flow measurements at the valve and flow meter, with the result that $FLOW_BLANK_{valve} = k_{cal} \cdot FLOW_BLANK_{flow\ meter}$.

2.3.2. Sorption Mode Protocol

The thermostatic bath was pre-heated at 308 K. At t_0 , the A-vessel rotation speed was set at 120 rpm and the system “A-vessel + amine” was submerged into the thermostatic bath. Simultaneously, a flow (L/min; normalized to room pressure) of CO₂ was conveyed through a pipe to the A-vessel. The CO₂ flow at the inlet of the reactor was both controlled

and recorded by the valve, while the CO₂ flow at the outlet was recorded by the flow meter. CO₂ sorption step duration was set to be equal to 6 min. At $t = 6$ min, the A-vessel was removed from the thermostatic bath and separated from the distiller rotating arm. The vessel's external walls were dried, and the system composed of "A-vessel + amine + CO₂" was equilibrated at room temperature and weighed, thus enabling the determination of the carbon dioxide mass trapped within. EC and pH were systematically measured after each sorption and desorption step. The system "A-vessel + amine + CO₂" was then reassembled with the distiller. The valve was closed, and the experimental setup was switched to the desorption mode.

2.3.3. Desorption Mode Protocol

The thermostatic bath was pre-heated at a given temperature (308, 323, 333, 343, 353 and 363 K). At t_0 , the A-vessel rotation speed was set at 120 rpm and the "A-vessel + amine + CO₂" system was immersed into the heated thermostatic bath; every desorption step lasted 10 min. At t_0 , the flow meter and the pressure meter data acquisition started, and the diaphragm pump was turned on. The internal pressure P_0 of the reactor was recorded by the pressure meter. At $t = 10$ min, the B-vessel was removed from the distiller column. The A-vessel was also removed from the thermostatic bath and separated from the distiller's rotating arm. The vessel's external walls were dried and the whole "A-B-vessels + amine + CO₂" was equilibrated at room temperature and weighed. In so doing, we were able to determine initial and final CO₂ concentrations in the sample, accounting also for the average weight loss established by the "blank" experiments, as stated above. The distillate was then transferred from the B-vessel to A-vessel to produce a homogeneous solution, and both vessels were reassembled with the distiller. The valve was opened to switch back the system to the sorption.

2.3.4. Data Treatment

As stated in Section 2.3.2, valve and flow meter allowed us to measure the CO₂ flows at the inlet and outlet of the reactor, respectively. In doing so, the instantaneous sorption rate as a function of time $\eta(t)_j$ at the j th-cycle was calculated, according to the equation:

$$\eta(t)_j = 100 \times \left(1 - \frac{k_{cal} \times \mu(t)_{sor,j}}{B(t)_j} \right) \quad (2)$$

where $B(t)$ (L/min) = mass stream recording of the inflow (sorption mode); $\mu(t)_{sor}$ (L/min) = flow meter recording of the outflow (sorption mode); and k_{cal} : calibration factor defined in Section 2.3.1. Note that η includes the fractions of CO₂ that are either actually sorbed by amine or dissolved into the active solution. The average of Equation (2) over N cycles is given by Equation (3)

$$\eta(t) = \frac{1}{N} \sum_{j=1}^N \eta(t)_j \quad (3)$$

Note that, in addition to $\mu(t)_{sor}$, we also introduce the outflow in desorption mode, i.e., $\mu(t)_{des}$, which is used to investigate the desorption kinetics.

$V_{CO_2\ sor,j}$ and $V_{CO_2\ des,j}$ are the sorbed and desorbed CO₂ volumes at room pressure over the sorption ($\Delta t_{sor,j}$) and desorption ($\Delta t_{des,j}$) j th-step, calculated using the following equations:

$$V_{CO_2\ sor,j} = \int_0^{\Delta t_{sor,j}} \eta(t')_j \times B(t')_j dt' \quad (4)$$

and

$$V_{CO_2\ des,j} = \int_0^{\Delta t_{des,j}} \mu(t')_j des dt' \quad (5)$$

The averages over the full series of 10 cycles of the quantities calculated by Equations (4) and (5) are referred to by $\bar{V}_{CO_2 sor}$ and $\bar{V}_{CO_2 des}$, i.e.,

$$\bar{V}_{CO_2 sor} = \frac{1}{N} \sum_{j=1}^N V_{CO_2 sor,j} \quad (6)$$

and

$$\bar{V}_{CO_2 des} = \frac{1}{N} \sum_{j=1}^N V_{CO_2 des,j} \quad (7)$$

The raw CO₂ mass transfer, ω_{CO_2} , is defined by the equations

$$\omega_{CO_2 sor,j} = m_{sor,j} - m_{des,j-1} \quad (8)$$

and

$$\omega_{CO_2 des,j} = m_{des,j} - m_{des,j} \quad (9)$$

where $m_{sor,j}$ and $m_{des,j}$ are the active solution's masses measured after sorption and desorption, at the j th-cycle, respectively.

The average exchange capacity, $\bar{\Delta\omega}$, is given by

$$\bar{\Delta\omega} = \frac{\sum_{j=1}^N \omega_{CO_2 des,j}}{\sum_{j=1}^N \omega_{CO_2 sor,j}} \times 100 \quad (10)$$

Eventually, we introduce CO₂ loading, a_j (mol/kg), defined as the net CO₂ moles in the sample per active solution mass unity at the j th-cycle of sorption/desorption, i.e.,

$$a_j = \frac{m_{sor/des,j}}{M_{CO_2} \times m_0} \quad (11)$$

where $m_{sor/des,j}$ = net mass of CO₂ trapped in the system, M_{CO_2} = CO₂ molar mass and m_0 = initial mass of the active solution, at the j th cycle.

The residual CO₂ loading, i.e., $Res(t)$, has been calculated upon desorption by the relationship reported below:

$$Res(t) = \bar{a}_{sor} - \frac{\int_0^t \mu_{des}(t') dt'}{\int_0^\infty \mu_{des}(t') dt'} \times \bar{\Delta a} \quad (12)$$

where: $\bar{\Delta a}$ = average $\langle a_{sor,j} - a_{des,j} \rangle_j$ over sorption/desorption cycles; \bar{a}_{sor} = average of the CO₂ loading after sorption.

3. Results

3.1. Sorption–Desorption Cycles' General Characterization

Figure 3A provides a visual representation of the sorption–desorption cycles' behavior in terms of CO₂ loading. Only experiments A1, A3 and A6, conducted at 308 K, 333 K and 363 K, respectively, are shown, as they represent average and extreme desorption temperatures. The CO₂ loading/unloading cycles show a trend characterized by “oscillations”, reflecting the processes of trapping/releasing carbon dioxide. The amplitude of each oscillation is related to the desorption temperature. This is in keeping with the CO₂ exchange capacity, $\bar{\Delta\omega}$ of Equation (10), which increases linearly with desorption temperature (Figure 3B). The relevant effect of the desorption temperature on the CO₂ exchange capacity is made apparent by the fact that a ΔT -change < 60 K, from 308 to 363 K, yields an increase in $\bar{\Delta\omega}$ from ~20 to about 99%, hinting at a very low degree of active solution degradation within the explored operating conditions.

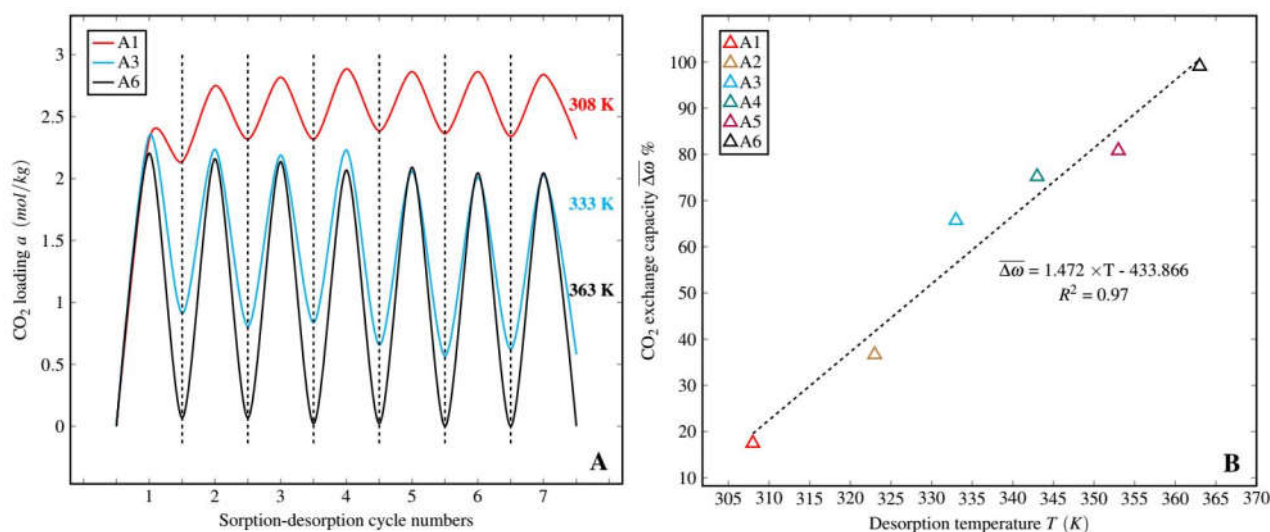


Figure 3. CO₂ loading a (mol/kg) variations, from Equation (11), as a function of the sorption–desorption cycles (A); for the sake of simplicity, only experiments referring to the first 7 cycles out of 10 and related to A1, A3 and A6 of Table 1 are shown. The CO₂ exchange capacity $\Delta\bar{w}$ as a function of the desorption temperature (B).

The average over the A-experiments of the sorption cycle at 308 K is reported by Figure 4. The low value of the standard deviation indicates the high repeatability of such a process. $\eta(t)$ decreases with time, as expected, because of the progressive saturation of the amine’s capacity to sorb CO₂. Saturation is predicted to take place at about 510–520 s, from extrapolation of the quasi-linear trend shown in Figure 4 for sorption time >360 s.

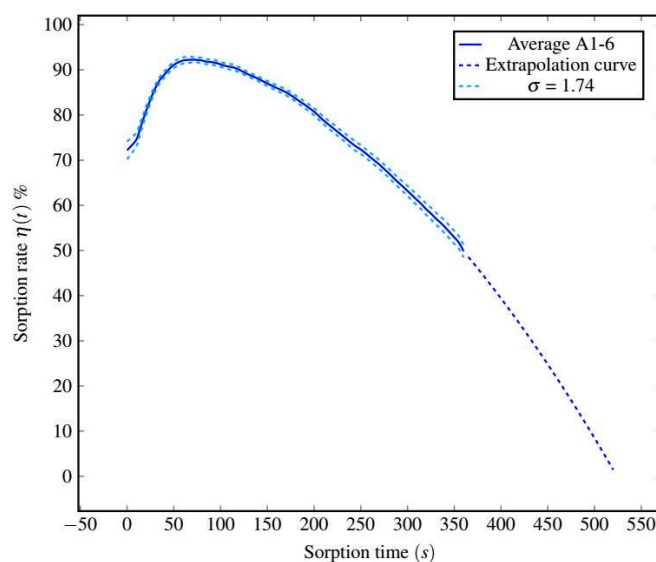


Figure 4. Average CO₂ sorption rate, calculated over experiments A1–A6 according to Equation (1) and related to the first cycle only, with standard deviation.

3.2. Kinetics

3.2.1. Experimental Results

The sorption rate, $\eta(t)$, and desorption flow, $\mu(t)_{des}$, are plotted in Figure 5 in the T -range of 308 to 363 K. Table 2 reports the related average sorption and desorption volumes, $\bar{V}_{CO_2 sor}$ (Equation (4)) and $\bar{V}_{CO_2 des}$ (Equation (5)), respectively. We introduce $\bar{\mu}(t \leq 150)$, i.e., the average desorption outflow at a low desorption time, as most of the desorption reaction occurs over the 0–150 s interval. Additionally, we also define the “average mass differentiation”,

\bar{m}_{diff} , corresponding to the mean fraction of amine mass transferred from vessel-A to vessel-B (Figure 2), during desorption, i.e., $\bar{m}_{\text{diff}} = \langle m_{\text{vessel-B}}/m_{\text{vessel-A+CO}_2} \rangle \times 100$.

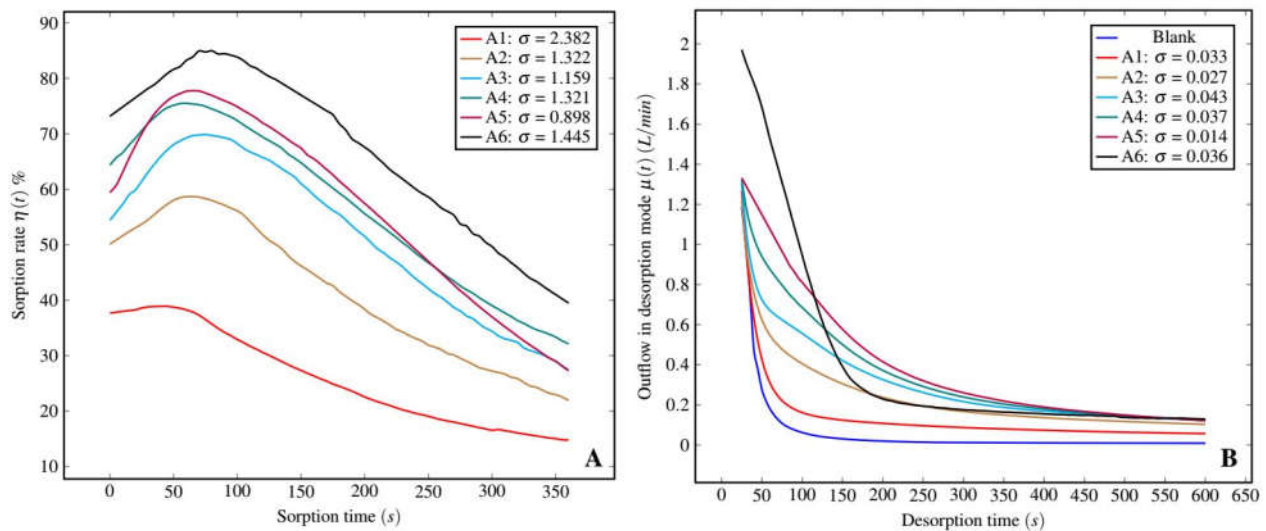


Figure 5. Average CO₂ sorption rate (A) and CO₂ desorption flow (L/min CO₂; B), as a function of the sorption/desorption time respectively, with the standard deviations σ , for experiments A1 to A6.

Table 2. CO₂ sorbed and desorbed volumes, $\bar{V}_{\text{CO}_2 \text{ sor}}$ (L/cycle) and $\bar{V}_{\text{CO}_2 \text{ des}}$ (L/cycle); $\bar{\mu}_{\text{des}}$ ($t \leq 150$ s) average $\mu_{\text{des}}(t)$ at low desorption time; mass differentiation, \bar{m}_{diff} (wt.%), between vessels A and B.

Experiment		A1	A2	A3	A4	A5	A6
$\bar{V}_{\text{CO}_2 \text{ sor}}$	(L·cycle ⁻¹)	0.98	1.86	2.31	2.77	3.08	3.28
$\bar{V}_{\text{CO}_2 \text{ des}}$	(L·cycle ⁻¹)	0.81	1.74	2.25	2.75	3.07	3.27
$\bar{V}_{\text{CO}_2 \text{ sor}}/\bar{V}_{\text{CO}_2 \text{ des}}$		1.21	1.07	1.03	1.01	1.00	1.00
$\bar{\mu}_{\text{des}}(t \leq 150)$	(L·min ⁻¹)	0.12	0.26	0.33	0.39	0.54	0.82
\bar{m}_{diff}	(wt.%)	0	0	0	0.35	0.8	47.4

In general, the η -curves of Figure 5A exhibit similar trends, i.e., a $\eta(t)$ increase is followed by a quasi-linear decrease, thus illustrating that the rate of reaction slows down as the CO₂ loading in the solution increases and the concentration of CO₂-free amine [Am_f] decreases. $\eta(t)$ depends on the efficiency of the preceding desorption process, which, in turn, is affected by the temperature used for boosting desorption.

Likewise, all of the μ_{des} -curves share qualitatively similar patterns. The μ_{des} -average over the 0–150 s interval ranges between 0.12 and 0.82 L/min. Note that the desorption process at 363 K exhibits a trend that, although it is in general coherence with those of the other isotherms, still displays differences. This reflects the substantial increase in the differentiation of the liquid phase, i.e., \bar{m}_{diff} , that passes from, 0.8 wt.% at 353 K to 47.4 wt.% at 363 K, the latter value corresponding to the boiling point of water at $p = 700$ mbar. This sharp increase is related to the substantial sample evaporation occurring primarily at a short desorption time ($t < 150$ s) and leading to fast CO₂ desorption driven by thermal effects. The latter yields an increase in the molecular mobility of CO₂ at a high temperature and a concurrent increase in the CO₂ concentration in the liquid phase due to sample evaporation.

The joint effects of pressure and temperature on desorption kinetics are displayed by Figure 6, in which the $\Delta\mu(t)$ curve of the experimental series A and B, i.e.,

$$\Delta\mu(t) = \mu(t)_{323-363 \text{ K}; P} - \mu(t)_{308 \text{ K}; P_0} \quad (13)$$

are shown.

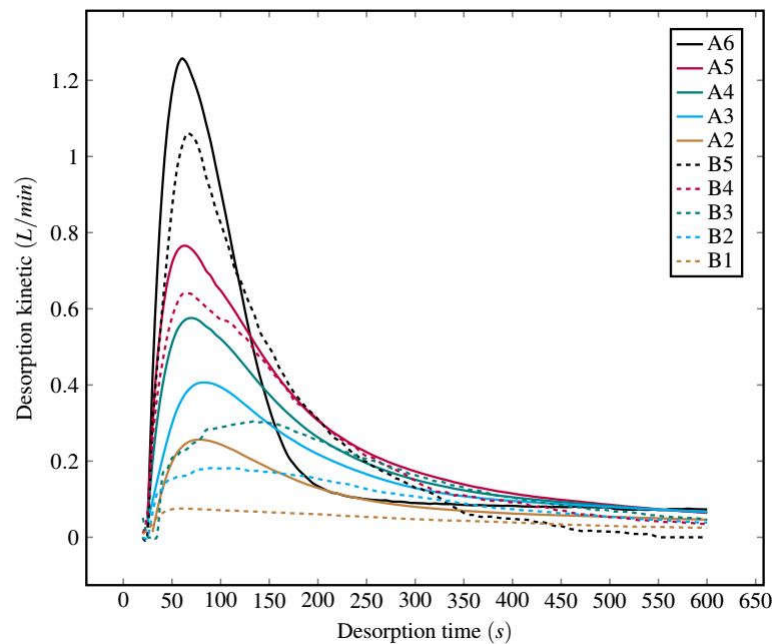


Figure 6. Pressure effect on desorption kinetics, using $\Delta\mu$ as defined in the text from the experimental series A and B.

A reduction in pressure leads to a general acceleration of the desorption kinetics, thus allowing for a thermal energy saving to break the adsorbent–adsorbate bonds. On average, a pressure reduction (1 bar \rightarrow \sim 0.2 bar) boosts desorption by \sim 16.3% at 363 K, up to \sim 70.5% at 323 K (calculations from Figure 6), in keeping with the observations of [25].

3.2.2. Desorption Kinetics Modeling

The Avrami–Erofeyev model [26] was fitted to the desorption data [17,27–29] and we used Equation (14) to define the following conversion variable

$$\alpha(t) = \frac{\int_0^t \mu_{des}(t') dt'}{\int_0^\infty \mu_{des}(t') dt'} \quad (14)$$

where $\lim_{t \rightarrow 0} \alpha = 0$ and $\lim_{t \rightarrow \infty} \alpha = 1$, i.e., at infinite time, desorption has ideally achieved its full completion.

α , in turn, relates to the Avrami kinetic parameters m and k in terms of

$$\alpha(t) = 1 - \exp(-(k t)^m) \quad (15)$$

Figure 7 displays $\alpha(t)$, for the experimental series A1–A6; the parameters m and k of Equation (15) are set out in Table 3.

Note that the value of m lies in the interval 0.469–0.781, thus suggesting that different desorption mechanisms occurred. Furthermore, these results suggest a possible associated with physical desorption and chemical desorption, as proposed by [28]. The value of m increases with T , which is consistent with a faster chemical desorption induced by temperature, but for A6. In such a case, the increase in m is related to the rapid water evaporation observed at low desorption time (see value of \bar{m}_{diff} in Table 2), inducing a faster physical desorption reaction, as proven by k .

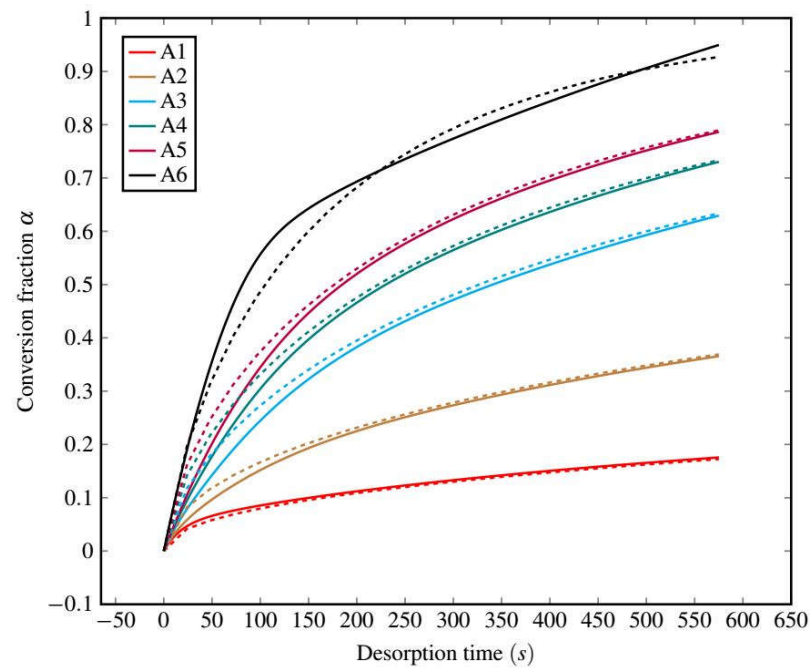


Figure 7. α as a function of t (s), in the thermal range from 308 to 363 K. The Avrami–Erofeev model interpolation curves are shown (dashed lines) with observations (solid lines).

Table 3. Order parameter m with the corresponding k and R^2 values.

Experiments	A1	A2	A3	A4	A5	A6
m	0.469	0.529	0.655	0.679	0.686	0.781
k (min^{-1})	$5.01 \cdot 10^{-5}$	$4.02 \cdot 10^{-4}$	$1.75 \cdot 10^{-3}$	$2.62 \cdot 10^{-3}$	$3.32 \cdot 10^{-3}$	$5.97 \cdot 10^{-3}$
R^2	0.9997	0.9998	0.9997	0.9998	0.9998	0.9728

Using the Arrhenius model, we plot $\ln(k)$ as a function of $1/T$ in order to infer the classical parameters A and E_A according to the equation below

$$k(T) = Ae^{-\frac{E_A}{RT}} \quad (16)$$

and visually displayed by Figure 8.

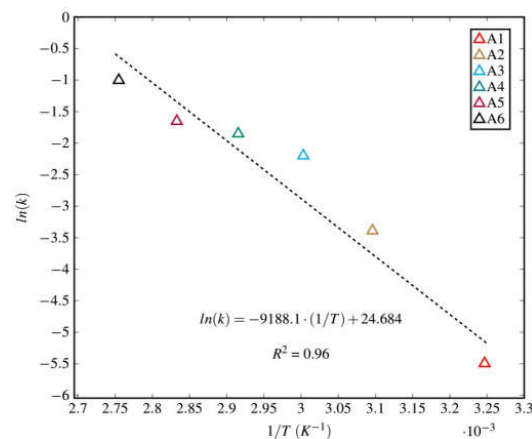


Figure 8. Arrhenius plots for the kinetic constants obtained by the Avrami–Erofeev model of desorption.

A and E_A are determined to be as large as $5.25 \cdot 10^{10} \text{ s}^{-1}$ and 76.4 kJ mol^{-1} , respectively. Such an E_A figure is in good agreement with those previously observed by [30], such as

an MDEA-based amine blend at ambient pressure conditions ranging between 50 and 85 kJ mol⁻¹.

Figure 9 illustrates the decrease in residual CO₂ loading Res as a function of desorption time, calculated using Equation (12).

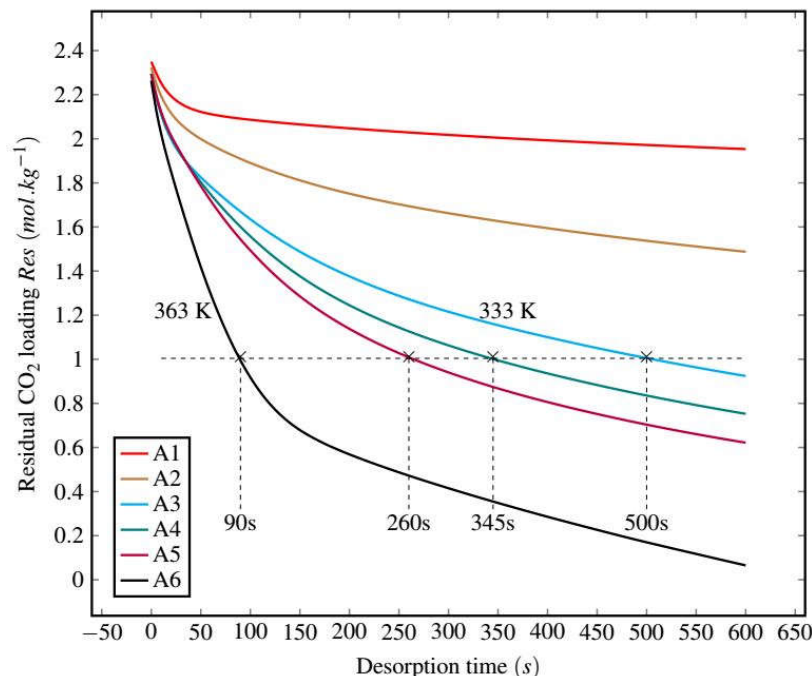


Figure 9. Decrease in residual CO₂ loading Res (mol kg⁻¹) as a function of desorption time (s) with the corresponding duration required to achieve 1 mol kg⁻¹.

The analysis quantifies the diminishing time required to reduce the CO₂ loading from its initial maximum value (in the range 2.34–2.26 mol kg⁻¹) to a common reference of 1 mol kg⁻¹ as the temperature increases. At 333 K, it takes 500 s to reach this reference value. Conversely, at temperatures of 343 K, 353 K, and 363 K, it takes 345 s, 260 s, and 90 s, respectively. For lower temperatures, the threshold of 1 mol kg⁻¹ was not reached within the limited desorption time. However, at 308 K and 323 K, after 600 s of desorption, the CO₂ loadings still reduces at 1.95 mol kg⁻¹ and 1.49 mol kg⁻¹, respectively.

4. Conclusions

The present study contributes to shedding light on the desorption kinetics of the CO₂ removal process using MDEA/PZ under simulated sorption/desorption cycles. We examined the desorption behavior at low pressures (<200 mbar) and within a temperature range of 308 to 363 K by employing a roto-evaporator system.

Our findings reveal that the combination of pressure and temperature significantly influences desorption reactions. Notably, at low pressure (~200 mbar), we observed a substantial enhancement in CO₂ extraction, with improvements of up to 70.5% at 323 K and 16.3% at 363 K compared to room pressure, as illustrated in Figure 6. This suggests that pressure reduction could serve as a promising alternative to high-temperature regeneration in the CO₂ removal process.

Furthermore, the application of the Arrhenius law to analyze the desorption process in the low-pressure regime yielded an activation energy of $E_A = 76.39$ kJ mol⁻¹, underscoring the relevant temperature sensitivity of this process. The analysis of the time required to decrease the CO₂ loading from its maximum value to a common reference (1 mol kg⁻¹) using Equation (12) demonstrates that 500 s is needed at 333 K vs. 90 s at 363 K, as displayed by Figure 9. These rapid desorption kinetics have practical implications for the design of

industrial CO₂ removal and transportation systems, particularly in scenarios where short residence times in terms of the stripper are necessary due to high reagent flow velocities.

Importantly, our study demonstrates that, if an industrial CO₂ stripping system can accommodate longer residence times, sufficient CO₂ desorption kinetics can still be achieved by reducing the desorption temperature to 333 K, balancing the trade-off between energy consumption and desorption performance.

Overall, the findings presented in this study contribute to a better understanding of desorption kinetics in the context of CO₂ removal processes. The insights gained have implications for the optimization of industrial CO₂ capture systems, promoting sustainability by enabling more efficient approaches to CO₂ removal and transportation.

Author Contributions: Conceptualization, Q.W., E.D., A.P., A.D.R. and A.M.V.; methodology, Q.W. and E.D.; investigation, Q.W., E.D. and L.P.; resources, Q.W., E.D., C.C., L.P., A.P., A.D.R. and A.M.V.; data curation, Q.W., E.D. and C.C.; writing—original draft preparation, Q.W., E.D., C.C. and A.P.; writing—review and editing, Q.W., E.D., C.C., L.P., D.B., M.B., A.B., A.P., A.D.R. and A.M.V.; visualization, Q.W.; supervision, E.D., C.C. and A.P.; project administration, A.P.; funding acquisition, A.P. All authors have read and agreed to the published version of the manuscript.

Funding: This research was funded by ECOSPRAY TECHNOLOGIES S.r.l., Italian Ministry for Education, University and Research (MIUR; project PRIN2017-2017L83S77) and Ministry for Ecological Transition (MiTE; project CLEAN), for possible applications of exchanged CO₂ to fly ash treatment.

Institutional Review Board Statement: Not applicable.

Informed Consent Statement: Not applicable.

Data Availability Statement: Derived data supporting the findings of this study are available from the corresponding author Q.W. on request.

Conflicts of Interest: The authors declare no conflict of interest. The funders had no role in the design of the study; in the collection, analyses, or interpretation of data; in the writing of the manuscript, or in the decision to publish the results; they provided the samples only.

References

1. Gür, T.M. Carbon dioxide emissions, capture, storage and utilization: Review of materials, processes and technologies. *Prog. Energy Combust. Sci.* **2022**, *89*, 100965. [[CrossRef](#)]
2. Aghel, B.; Janati, S.; Wongwises, S.; Shadloo, M.S. Review on CO₂ capture by blended amine solutions. *Int. J. Greenh. Gas Control* **2022**, *119*, 103715. [[CrossRef](#)]
3. Barzagli, F.; Giorgi, C.; Mani, F.; Peruzzini, M. Reversible carbon dioxide capture by aqueous and non- aqueous amine-based absorbents: A comparative analysis carried out by ¹³C NMR spectroscopy. *Appl. Energy* **2018**, *220*, 208–219. [[CrossRef](#)]
4. Khalid, M.; Dharaskar, S.A.; Sillanpaa, M.; Siddiqui, H. (Eds.) *Emerging Carbon Capture Technologies: Towards a Sustainable Future*; Elsevier: Amsterdam, The Netherlands, 2022.
5. Closmann, F.; Nguyen, T.; Rochelle, G.T. MDEA/Piperazine as a solvent for CO₂ capture. *Energy Procedia* **2009**, *1*, 1351–1357. [[CrossRef](#)]
6. Dugas, R.; Rochelle, G. Absorption and desorption rates of carbon dioxide with monoethanolamine and piperazine. *Energy Procedia* **2009**, *1*, 1163–1169. [[CrossRef](#)]
7. Svensson, H.; Hultberg, C.; Karlsson, H.T. Heat of absorption of CO₂ in aqueous solutions of N-methyldiethanolamine and piperazine. *Int. J. Greenh. Gas Control* **2013**, *17*, 89–98. [[CrossRef](#)]
8. Artanto, Y.; Jansen, J.; Pearson, P.; Do, T.; Cottrell, A.; Meuleman, E.; Feron, P. Performance of MEA and amine-blends in the CSIRO PCC pilot plant at Loy Yang Power in Australia. *Fuel* **2012**, *101*, 264–275. [[CrossRef](#)]
9. Yan, S.; Fang, M.; Luo, Z.; Cen, K. Regeneration of CO₂ from CO₂-rich alkanolamines solution by using reduced thickness and vacuum technology: Regeneration feasibility and characteristic of thin-layer solvent. *Chem. Eng. Process. Process Intensif.* **2009**, *48*, 515–523. [[CrossRef](#)]
10. Fredriksen, S.; Jens, K.-J. Oxidative degradation of aqueous amine solutions of MEA, AMP, MDEA, Pz: A review. *Energy Proc.* **2013**, *37*, 1770–1777. [[CrossRef](#)]
11. Zhang, W.; Liu, H.; Sun, Y.; Cakstins, J.; Sun, C.; Snape, C.E. Parametric study on the regeneration heat requirement of an amine-based solid adsorbent process for post-combustion carbon capture. *Appl. Energy* **2016**, *168*, 394–405. [[CrossRef](#)]
12. Abd, A.A.; Naji, S.Z.; Barifcani, A. Comprehensive evaluation and sensitivity analysis of regeneration energy for acid gas removal plant using single and activated-methyl diethanolamine solvents. *Chin. J. Chem. Eng.* **2020**, *28*, 1684–1693. [[CrossRef](#)]

13. Li, F.; Hemmati, A.; Rashidi, H. Industrial CO₂ absorption into methyldiethanolamine/piperazine in place of monoethanolamine in the absorption column. *Process Saf. Environ. Prot.* **2020**, *142*, 83–91. [[CrossRef](#)]
14. Hemmati, A.; Farahzad, R.; Surendar, A.; Aminahmadi, B. Validation of mass transfer and liquid holdup correlations for CO₂ absorption process with methyldiethanolamine solvent and piperazine as an activator. *Process Saf. Environ. Prot.* **2019**, *126*, 214–222. [[CrossRef](#)]
15. Esmaeili, A.; Tamuzi, A.; Borhani, T.N.; Xiang, Y.; Shao, L. Modeling of carbon dioxide absorption by solution of piperazine and methyldiethanolamine in a rotating packed bed. *Chem. Eng. Sci.* **2022**, *248*, 117118. [[CrossRef](#)]
16. Barzagli, F.; Mani, F.; Peruzzini, M. Continuous cycles of CO₂ absorption and amine regeneration with aqueous alkanolamines: A comparison of the efficiency between pure and blended DEA, MDEA and AMP solutions by ¹³C NMR spectroscopy. *Energy Env. Ment. Sci.* **2010**, *3*, 772–779. [[CrossRef](#)]
17. Teng, Y.; Liu, Z.; Xu, G.; Zhang, K. Desorption kinetics and mechanisms of CO₂ on amine-based mesoporous silica materials. *Energies* **2017**, *10*, 115. [[CrossRef](#)]
18. Zhang, X.; Zhang, C.-F.; Qin, S.-J.; Zheng, Z.-S. A kinetics study on the absorption of carbon dioxide into a mixed aqueous solution of methyldiethanolamine and piperazine. *Ind. Eng. Chem. Res.* **2001**, *40*, 3785–3791. [[CrossRef](#)]
19. Bishnoi, S.; Rochelle, G.T. Absorption of carbon dioxide into aqueous piperazine: Reaction kinetics, mass transfer and solubility. *Chem. Eng. Sci.* **2000**, *55*, 5531–5543. [[CrossRef](#)]
20. Puxty, G.; Rowland, R. Modeling CO₂ mass transfer in amine mixtures: PZ-AMP and PZ-MDEA. *Environ. Sci. Technol.* **2011**, *45*, 2398–2405. [[CrossRef](#)]
21. Jansen, D.; Gazzani, M.; Manzolini, G.; van Dijk, E.; Carbo, M. Pre-combustion CO₂ capture. *Int. J. Greenh. Gas Control* **2015**, *40*, 167–187. [[CrossRef](#)]
22. Chen, C.; Zhang, S.; Row, K.H.; Ahn, W.-S. Amine–silica composites for CO₂ capture: A short review. *J. Energy Chem.* **2017**, *26*, 868–880. [[CrossRef](#)]
23. Sun, Z.; Fan, M.; Argyle, M. Desorption kinetics of the monoethanolamine/macroporous TiO₂-based CO₂ separation process. *Energy Fuels* **2011**, *25*, 2988–2996. [[CrossRef](#)]
24. Saleh, T.A.; Elsharif, A.M.; Bin-Dahman, O.A. Synthesis of amine functionalization carbon nanotube-low symmetry porphyrin derivatives conjugates toward dye and metal ions removal. *J. Mol. Liq.* **2021**, *340*, 117024. [[CrossRef](#)]
25. Zhang, J.; Qiao, Y.; Agar, D.W. Intensification of low temperature thermomorphic biphasic amine solvent regeneration for CO₂ capture. *Chem. Eng. Res. Des.* **2012**, *90*, 743–749. [[CrossRef](#)]
26. Khawam, A.; Flanagan, D.R. Solid-state kinetic models: Basics and mathematical fundamentals. *J. Phys. Chem. B* **2006**, *110*, 17315–17328. [[CrossRef](#)]
27. Guo, B.; Wang, Y.; Shen, X.; Qiao, X.; Jia, L.; Xiang, J.; Jin, Y. Study on CO₂ capture characteristics and kinetics of modified potassium-based adsorbents. *Materials* **2020**, *13*, 877. [[CrossRef](#)]
28. Liu, Q.; Shi, J.; Zheng, S.; Tao, M.; He, Y.; Shi, Y. Kinetics studies of CO₂ adsorption/desorption on amine-functionalized multiwalled carbon nanotubes. *Ind. Eng. Chem. Res.* **2014**, *53*, 11677–11683. [[CrossRef](#)]
29. Serna-Guerrero, R.; Belmabkhout, Y.; Sayari, A. Modeling CO₂ adsorption on amine-functionalized mesoporous silica: 1. A semi-empirical equilibrium model. *Chem. Eng. J.* **2010**, *161*, 173–181. [[CrossRef](#)]
30. Shunji, K.; Xizhou, S.; Wenze, Y. Investigation of CO₂ desorption kinetics in MDEA and MDEA+ DEA rich amine solutions with thermo-gravimetric analysis method. *Int. J. Greenh. Gas Control* **2020**, *95*, 102947. [[CrossRef](#)]

Disclaimer/Publisher’s Note: The statements, opinions and data contained in all publications are solely those of the individual author(s) and contributor(s) and not of MDPI and/or the editor(s). MDPI and/or the editor(s) disclaim responsibility for any injury to people or property resulting from any ideas, methods, instructions or products referred to in the content.